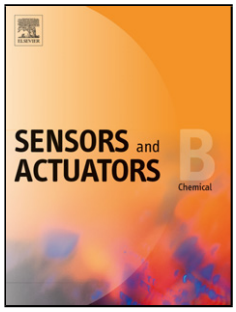

Title: Impedimetric fingerprinting and structural analysis of isogenic *E. coli* biofilms using multielectrode arrays

Authors: Erkuden Goikoetxea, Denis Routkevitch, Ami de Weerdt, Jordan J. Green, Hans Steenackers, Dries Braeken

PII: S0925-4005(18)30212-0
DOI: https://doi.org/10.1016/j.snb.2018.01.188
Reference: SNB 24037

To appear in: *Sensors and Actuators B*

Received date: 30-11-2017
Accepted date: 24-1-2018

Please cite this article as: Erkuden Goikoetxea, Denis Routkevitch, Ami de Weerdt, Jordan J.Green, Hans Steenackers, Dries Braeken, Impedimetric fingerprinting and structural analysis of isogenic E.coli biofilms using multielectrode arrays, Sensors and Actuators B: Chemical https://doi.org/10.1016/j.snb.2018.01.188

Title: Impedimetric fingerprinting and structural analysis of isogenic *E. coli* biofilms using multielectrode arrays

Author names and affiliations:

Erkuden Goikoetxea[1,2], Denis Routkevitch[3], Ami de Weerdt[1], Jordan J. Green[3], Hans Steenackers[1*], Dries Braeken[2*]

[1] Centre of Microbial and Plant Genetics, Department of Microbial and Molecular Systems, KU Leuven, Leuven, Belgium

[2] Life Sciences & Imaging Department, imec, Kapeldreef 75 Heverlee, Belgium

[3] Ophthalmology, Oncology, Neurosurgery, and Materials Science & Engineering at the Johns Hopkins University School of Medicine

*Corresponding authors: Hans.Steenackers@biw.kuleuven.be; Dries.Braeken@imec.be

Research highlights

- We discriminated between isogenic biofilms based on specific impedance profiles.
- Biofilms producing curli protein showed an increased interfacial resistance.
- The WT biofilm showed the largest impedance heterogeneity.
- The attachment phase showed an initial increase in interfacial resistance.
- During the biofilm maturation phase we observed a decrease in medium resistance.

Abstract

Microbial biofilm contamination is an ubiquitous and persistent problem in industry and clinics. The structure of the biofilm, its extracellular matrix and its formation process are very complex. At present, there are only limited options to investigate biofilms outside the lab, as most *in situ* techniques lack sensitivity and resolution. Impedance-based sensors provide a fast, label-free and sensitive manner to characterize biofilms, although mainly large electrodes have been used so far. Here, we used 60 µm-sized electrode arrays (MEAs) to characterize the structure of biofilms formed by wild type (WT) *Escherichia coli* TG1 and the isogenic *ΔcsgD*, *ΔcsgB* and *ΔbcsA* mutants. At 24h of growth, the interfacial resistance at 2Hz increased by 3.4% and 0.3% for the curli producing strains (WT and *ΔbcsA*), yet it decreased by 5.7% and 4% for the curli non-producing strains (*ΔcsgD* and *ΔcsgB)*. The imaginary impedance at 2Hz decreased for all the strains by 7.2%, 6.9%, 5.1% and 2.5% (WT, *ΔbcsA, ΔcsgB* and *ΔcsgD,* respectively). Interestingly, the variation of impedance within each biofilm, resulting from physiological heterogeneity, was significantly different for each biofilm and most pronounced in the WT. Depending on the strain, the biofilm attachment phase lasted between 6 and 10h, and was characterized by an increase in the interfacial resistance of up to 6% for the WT, 5.5% for *ΔcsgD,* 3.5% for *ΔcsgB* and 5% for *ΔbcsA, as* opposed to the decrease in medium resistance observed during the maturation phase. Overall, impedance-based MEA assays proved effective to differentiate between biofilms with varying structure, detect spatial diversity and explain biofilm life-cycle in terms of attachment and maturation.

1. Introduction

Bacteria embed themselves in a hydrated matrix of polysaccharides and proteins, forming a slimy layer known as a biofilm. Within such a protective layer, bacteria are up to one thousand times more tolerant to antimicrobials [1]. Bacterial biofilm contamination is therefore a common and persistent problem for industries such as the pharmaceutical sector, water treatment industry and the food and beverage industry [2]. In the medical sector biofilms are often associated with implant-related infections [3]. Some of the mechanisms that make biofilms so difficult to eradicate involve their strong attachment, heterogeneity of the composition, structure of the community and the tolerance developed due to stress responses [4].

Therefore, there is a large interest in the development of new techniques that allow for sensitive, cheap and *in situ* monitoring of biofilms [2]. In the past decades, several approaches have been proposed to monitor and characterize biofilm growth. Optical sensors for example have been used to determine the absorption and scattering of light due to biofilms. Although these sensors provide information on thickness and bacterial density, they lack specificity and do not report on physical structure [5–7]. Mechanical sensors based on quartz crystal microbalance on the other hand offer sensitive biofilm detection but they are limited to detecting the attached biomass and the adsorption of proteins [8,9]. Specificity could be improved by using portable hyperspectral sensors [10]. The disadvantage however is that they require optimization for different surfaces and are not easy to implement in *in vivo* (implants) applications.

Electrochemical impedance spectroscopy (EIS) is a highly sensitive and label-free technique to characterize (bio)physical processes at the substrate-biomaterial interface [11]. With EIS, small alternating voltages are applied and the resulting alternating current flows from a working electrode across the target sample to an opposite counter electrode [12]. This current is then measured and the impedance is calculated as the ratio between the applied voltage and the current.

In the last decade, a number of impedimetric biosensors that detect biofilm growth overtime have been reported. Some of these approaches were implemented in various experimental setups such as petri dishes [13] and microtitre plates [14], modified CDC reactors [15] and microfluidic chambers [16–18], while other reports performed the experiments in a rudimentary electrode chamber [19–21]. However, in these studies, researchers never exploited the obtained data to study the spatial structure of different biofilms, presumably because the electrodes used in these studies are typically very large (mm^2 range). In order to increase the spatial resolution, and thus facilitate the study of the biofilm spatial structure, microelectrode arrays (MEAs) can be used. These micro-fabricated chips are often used to detect electrical activity from dissociated cell cultures such as cardiac and neuronal cells, but also served to study the electrical impedance properties of eukaryotic cells and tissue [22–24].

Here, we present an impedance assay based on MEAs to characterize structural differences between bacterial biofilms. As a proof of concept, we cultured the wild type and the isogenic *ΔcsgD*, *ΔcsgB* and *ΔbcsA* mutants of the well-known *Escherichia coli* TG1 biofilm forming strain on impedance based MEAs and compared their structural compositions. The gene *csgD* encodes the biofilm master regulator and its deletion results in an inhibited biofilm in which the extracellular matrix production is overall disrupted. *CsgB* and *bcsA* are downstream genes involved in the production of curli and cellulose, respectively. As a consequence, these three mutants do not produce curli and/or cellulose and show a lower tolerance to common antimicrobial protocols [25,26]. By using impedance sensing in MEAs, we successfully differentiated between these biofilms with varying structures that are associated with antimicrobial tolerance, we detected different levels of spatial diversity for each strain and we were able to explain the biofilm life-cycle in terms of attachment and maturation.

2. Materials and methods

2.1 Bacterial cultures and biofilm formation

Overnight cultures of the *E.coli* TG1 wild type (WT) and isogenic *ΔcsgD*, *ΔcsgB* and *ΔbcsA* mutant strains were grown in LB medium at 37°C under shaking conditions. The overnight cultures were then adjusted to an optical density (OD; 600 nm) of 0.35, which corresponds to a density of approximately $3.5x10^8$ cells/ml. The overnight culture was centrifuged (2 minutes @ 4000rpm) and the cells were resuspended in TSB 1/20. Next, we diluted the culture 1:100 in TSB 1/20. Sterilized MEA chambers were then filled with 2.5ml of the diluted cell suspensions and biofilms were formed by incubating for 24 hours at 25°C.

2.2 Microelectrode array sensors

E.coli biofilms were cultured on microelectrode array chips (Fig.1A). The MEAs used in this paper were designed for combined electrical recording and optical stimulation [27]. The electrodes on these chips are perfectly suited for sensitive impedance measurements of bacterial biofilms as they have a low intrinsic impedance (measured in PBX 1x at 1kHz 10.65 ± 1.17 kΩ (mean ± SD)). Prior to each experiment the MEAs were conditioned (15' UV-O_3 treatment) and sterilized (30' in ethanol 70%).

2.3 Experimental setup for overtime biofilm impedance monitoring

We designed a multiplexer system to allow for automated and sequential impedance monitoring from 60 channels. Channel switching is operated by relays (coto 9001-05-01) which are controlled by a Digital input/output device (Agilent u2600 series). A software developed in Labview is used to synchronize channel switching and impedance measurements (Fig. 1B). Impedance measurements were performed using an Autolab PGSTAT302N (EcoChemie, The Netherlands) containing a FRA-2 module and connected to a custom-designed multiplexer. Chips were measured inside an incubator at 25°C. The amplitude of the AC input voltage was 100 mV peak-to-peak and the measured frequencies ranged from 1 to 100kHz. An external Pt coil was used as counter electrode (Fig. 1C).

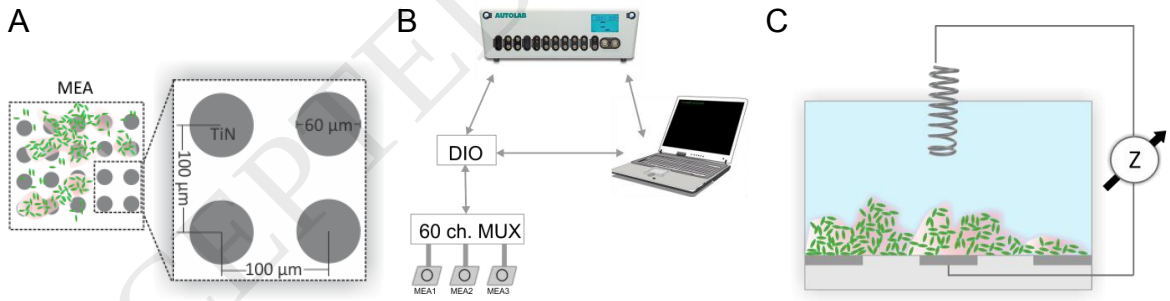

Figure 1. Illustration of the impedance measurement setup and layout of the microelectrode arrays. A) A subset of the MEA chip composed of 4x5 TiN electrodes of 60µm in diameter was used for the experiments. The pitch is 100µm in both directions. B) Schematic of the experimental setup. The system is designed for sequential impedance measurements of three MEA chips. C) Schematic representation of biofilm impedance chamber. Impedance is recorded between on-chip working electrodes and an external platinum coil electrode.

2.4 Confocal microscopy of bacterial biofilms

Biofilms were imaged by a Zen 780 confocal Laser Scanning Microscope (CLSM) with a 20x water immersion objective (Zeiss, Germany). Bacterial cells were electroporated with pFPV 25.1, a GFP encoding plasmid [28], and were excited with a 488 nm laser for fluorescence imaging. The extracellular matrix of the biofilms was stained by the polysaccharide binding conjugate of Alexa

Fluor633 and the lectin Concanavalin A (Molecular Probes, Belgium) and excited with a 633 nm laser. The single image thickness was set to 1 µm. The 3D visualization of the stacks was performed by the Volume Viewer plugin and the orthogonal views were processed with ImageJ.

2.5 SEM of bacterial biofilms

Biofilms were formed on TiN chips for 24 h as described in Section 2.1. After 24 h of biofilm growth the supernatants were removed and samples were subsequently fixed for 24 h at room temperature using a 4% paraformaldehyde fixation buffer. Next, the bacteria underwent post-fixation in a 2% osmium tetroxide (OsO_4) solution for 2 h, followed by dehydration using a series of increasing concentrations of ethanol (2 x 10 min of 20%, 40%, 60%, 80% and 95%, followed by 3 x 10 min of 100%). Lastly, the samples were dried using a liquid CO_2 critical point dryer (Automegasamdri-916B, Tousimis) and visualized using SEM (Nova NanoSEM 200, FEI).

2.6 Data pretreatment and analysis

Before analyzing the impedance of the individual electrodes from the MEA chips, we developed an outlier removal procedure to check for broken contacts. We analyzed the reference impedance values of the electrodes in sterile growth medium and we performed the Grubbs test at 1, 100 and 1kHz.

2.7 CFU count

To assess the number of viable cells embedded in the biofilm and floating in the supernatants we determined the colony forming units (CFU). The biofilms were cultured on TiN substrates chips in triplicate. After 24 hours ten-fold serial dilutions of the supernatants were plated out on agar plates to count the number of CFU's. Subsequently the biofilm cells on the MEAs were scraped off in 1 ml of PBS and the number of CFU's was determined by plate counting.

2.8 Statistical analysis

All data shown here were collected in triplicate. The differences between the impedance of the different strains were analyzed by one-way ANOVA with Bonferroni multiple comparisons correction. The differences between variances for each strain were analyzed by unequal variance unpaired t test (Welch). The growth curves were analyzed by linearly fitting the slope in the attachment and maturation phases.

3. Results and discussion

3.1 Impedimetric characterization of *E.coli* TG1 WT biofilms grown on MEAs

We used the *E. coli* TG1 strain as a model organism for impedimetric characterization of biofilms. Prior to assessment of the *E. coli* TG1 biofilm we characterized the impedance of the bare electrodes in sterile growth medium using a commercial impedance analyzer. As shown in Figure 2A-B (black trace), a frequency-dependent impedance profile was observed. Impedance is maximal in the low frequency (LF) region (1-100 Hz) and decreases with increasing frequency. The phase is close to -90°. Impedance in the LF region is generally dominated by the electrode-electrolyte capacitance and all surface related effects [29]. In the middle frequency (MF) region (100Hz to 50kHz) the magnitude shows a flat line and the phase is close to 0°. In this region the impedance is dominated by the resistance of the growth medium and all non-surface related effects [29]. In the high frequency (HF) region, the spectra are dominated by the unwanted stray capacitance of the system.

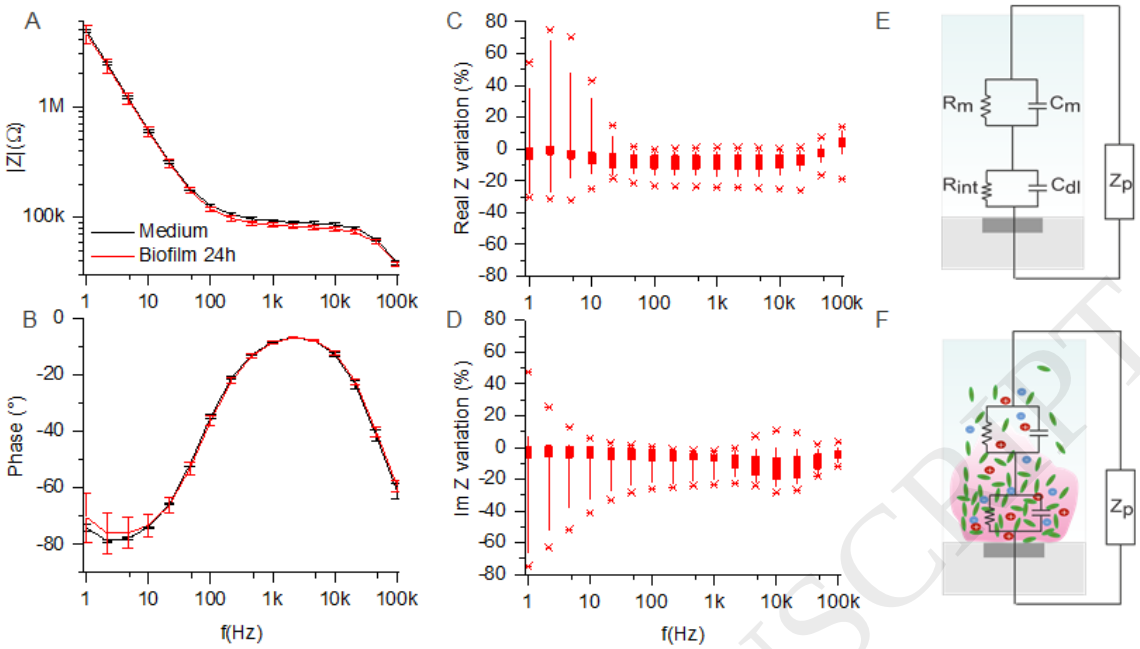

Figure 2. A-B. Impedance magnitude and phase of bare electrodes (black trace), *E. coli* WT biofilm after 24 hours of growth (red trace). Error bars correspond to ±1 SD, (3 MEAs, 20 electrodes each); C-D. Relative changes in the real and imaginary part of the impedance for biofilm-covered electrodes compared to the bare electrodes. The box covers 25-75% of the recorded electrodes and the whiskers 5-95%; E-F. Schematic drawing of the electrodes immersed in sterile growth medium and a biofilm grown on a MEA. The simplified equivalent circuit used for interpretation of the impedance of the bare electrodes as well as the biofilm is also depicted. R_{int} is the interfacial resistance, C_{dl} is the double layer capacitance and R_m and C_m are the medium resistance and capacitance, respectively. A biofilm culture consists of two phases, on the one hand, there is a biomass that consists of cells and metabolites embedded in polysaccharides attached to the electrodes. On the other hand, there are free-floating cells and metabolites in suspension.

After electrode characterization, we cultured the WT biofilm on the MEA surfaces for 24h and measured its impedimetric properties. On average, the biofilm growth on the electrodes results in a decrease in the magnitude of the impedance at 24h along the whole frequency spectrum (Fig. 2A, red trace).

In order to investigate the resistive and capacitive changes that the biofilm exerts on the impedance of the system we can treat this impedance as a vector, with a real (re) part and an imaginary (im) part, which are derived from the resistive and capacitive elements, respectively [29]. We calculated the percentile variation of the real and imaginary parts of the impedance (Fig. 2C and D, respectively) compared to the bare electrodes in sterile growth medium. In order to explain the effects at the electrode surface and in the supernatants we selected two different frequencies that are relevant for the changes on the electrode surface and in the supernatant. To do so we followed the reasoning elaborated before by Yang *et al.*[30]. In the low frequencies, i.e. LF= 2 Hz, we can detect changes on the electrode surface that are likely related to the cells growing on the surface and the extracellular matrix produced by these cells, whereas the middle frequencies, i.e. MF=5 kHz, are affected by changes in the supernatant related to planktonic cells and dissolved electrolytes. From here on we will refer to those parameters as LF_{re}, LF_{im} and MF_{re}, MF_{im} (see Table 1).

After 24 hours of growth, the LF_{re} increases with 14.8%. This can be explained by the insulating effect of the bacterial cells that are attached to the electrode. LF_{im} decreases by 8.5%, which is related to an increase in capacitive behaviour. This larger capacitance can be explained by changes in the permittivity on the electrode, which could be due to the presence of more polar molecules

compared to the situation before growth. Bacteria produce a number of charged molecules such as ammonia and acetate that change the ionic strength of the solution and therefore affect the double layer capacitance of the electrodes [31,32].

Similarly, we calculated the changes in the middle frequencies, caused by the cells and metabolites in the supernatant. The MF_{re} and the MF_{im} decrease by 8.7 and 12.3%, respectively. The decrease of MF_{re} is directly related to the increase of ionic strength of the medium [30,33].

3.2 Structural characterization of *ΔcsgD*, *ΔcsgB* and *ΔbcsA* mutants of *E. coli* TG1

Curli fimbriae proteins and cellulose fibers are the main extracellular components of *E. coli* and *Salmonella* biofilms and are involved in biofilm attachment and 3D structure development [34,35]. Moreover, they promote antimicrobial tolerance and make the biofilm more difficult to eradicate. *CsgD* encodes the master regulator of biofilm formation and knocking out this gene results in disruption of the biofilm structure by affecting both curli and cellulose production [36]. However, because of the presence of an independent, alternative pathway regulating cellulose production in *E. coli* biofilms [37], cellulose might still be produced to a certain extent. The mutants *ΔcsgB and ΔbcsA* on the other hand are only affected in curli and cellulose production, respectively. We selected the *ΔcsgD*, *ΔcsgB* and *ΔbcsA* mutants of *E. coli* TG1 in order to assess the influence of structural biofilm differences, associated with differential antimicrobial tolerance, on the impedance fingerprint. Visualization by scanning electron microscopy confirmed that there are clear differences between the WT and mutant biofilms. The WT biofilm is characterized by a higher number of attached cells and tower-like, multi-cellular aggregates. The mutants form thin, sparse biofilms with little cell attachment (Fig. 3A-D).

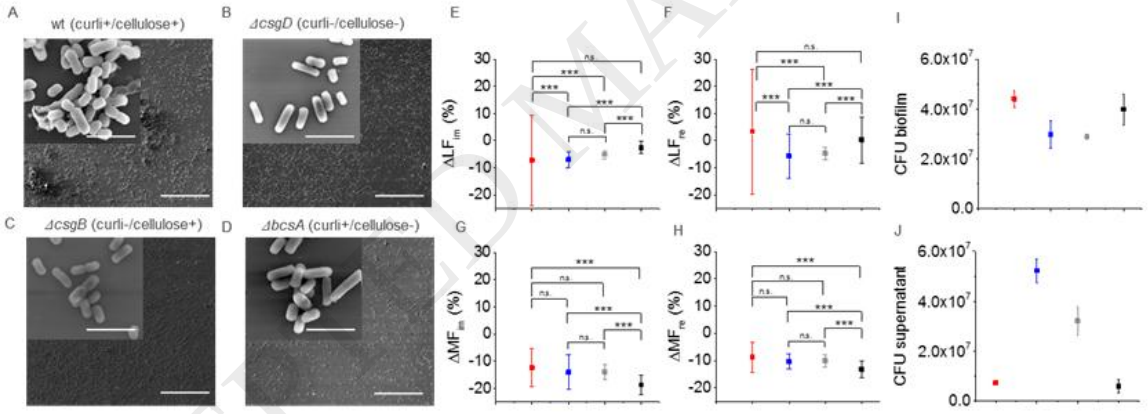

Figure 3. Structural characterization of WT (■), curli and cellulose deficient (*ΔcsgD* ■), curli deficient (*ΔcsgB* ■) and cellulose deficient (*ΔbcsA* ■) mutants; A-D. Scanning electron micrographs of WT and knock out mutants. Scale bar in inset is 1 µm and in the large image is 100 µm; E-H. Relative changes on changes on LF_{im}, LF_{re}, MF_{im} and MF_{re} (n=60 electrodes from 3 MEA chips); I –J. Colony forming units (CFU) for cells in the biofilm and in the supernatants (n=3 chips).

Identically to the WT biofilm characterization, we analyzed the relative changes in the real and imaginary part of impedance for the different mutant strains. We found that in the low frequency region of the impedance spectra (related to biofilm attachment), there is a significant difference in resistive (LF_{re}) and capacitive (LF_{im}) behavior between biofilms that express curli (WT and *ΔbcsA*) versus biofilms that lack these proteins (*ΔcsgB* and *ΔcsgD*). On the other hand, no significant differences were observed between WT (curli+/cellulose+) and *ΔbcsA* (curli+/cellulose-), neither between *ΔcsgD* (curli-/cellulose-) and *ΔcsgB* (curli-/cellulose+). This indicates that cellulose production itself cannot be discerned by analyzing LF parameters.

Like the wild type, all three mutants show a decrease in LF_{im}, which indicates an increase of the capacitance. This is in agreement with the reviewed literature where biofilm growth is directly related to increased capacitance. Paredes *et al.* detected a 40% increase in capacitance at 10 Hz after 24h of *Staphylococcus aureus* biofilm growth [15]. Similarly, Yang *et al.* observed a decrease in imaginary impedance at 1Hz of 4% [30]. They related the decrease in imaginary impedance to an increase in permittivity of the electrode double layer. The mature biofilms of curli-producing (WT and *ΔbcsA*) and curli-deficient strains (*ΔcsgB* and *ΔcsgD*) show a significantly different decrease in LF_{im} (7.2 ± 16.35% and 6.99 ± 2.8% for WT and *ΔcsgD* mutant, respectively). Further, it is worth mentioning that the variances for curli-producing and non-producing strains are significantly different. This variation results from the measurements at spatially different sites by the electrodes on the MEA, which is consistent with the higher heterogeneity of the curli-producing strains (see Fig. 3A-D, and Suppl. Fig. 1). Interestingly, WT and *ΔbcsA,* show an increase in apparent interfacial resistance (LF_{re}) on several electrodes up to 72% for the WT and 26% for the *ΔbcsA* mutant, whereas LF_{re} is decreased in the curli deficient mutants. Curli proteins promote cell attachment, which might block current and therefore increase the interfacial resistance. Both for LF_{im} and LF_{re} there were no significant differences observed between *ΔcsgD* and *ΔcsgB*. This result is consistent with both the appearance of the films which look very similar (confocal images in Suppl. Fig. 1B-C) as well as with the CFU count of the biofilm (Fig. 3 I). The curli producing biofilms, WT and *ΔbcsA*, are not significantly different either for the LF parameters. In addition, both biofilms show similar amounts of cells and they both formed thicker biofilms than the curli non producing strains (Suppl. Fig. 1A and D).

In the middle frequency (MF) region, related to the changes in the supernatant, we found that only the *ΔbcsA* mutant (curli+/cellulose-) is significantly different from the other strains. In the cell medium of this biofilm we observed macroscopically large, multi-cellular, floating turbid structures which we believe to have a significant effect on the impedance (Suppl. Fig. 2). The impedance changes in the middle frequency region could not be correlated to the cell counts in the supernatant. This suggests that the changes we measure using EIS are not affected by the amount of cells but rather by the metabolites. This observation is consistent with the work reported by Paredes *et al*. [38], Yang *et al.* [30] and Felice *et al.*[29].

Our biofilm assay consists of both attached biomass and free-living cells and metabolites in the medium, and both phases are in constant interplay. Therefore, the assay can be characterized by the proportion of surface to supernatant effects. In order to compare how the impedance for each biofilm is affected by the surface effects (LF) versus the supernatant (MF), we introduce the *biomass-planktonic state index* (BPI), which is defined as the mean of the absolute ratio between LF_{im} and MF_{im}. When the index is larger than 1, the surface effects dominate over the supernatant, and when the index is smaller than 1, there are more supernatant than surface effects. We found that for the WT biofilm this value is 1.47 (± 4.87) indicating that the impedance changes are dominated by the attached biomass. The same conclusion can be drawn from the colony forming units (CFU) evaluation of the chip surfaces (Figure 3I-J): the WT biofilm has most of its cells residing on the electrode surface. In contrast to the WT, the curli non-producing films (*ΔcsgD* and *ΔcsgB*) have most of the cells in the free-living state, and consistently their BPIs are smaller than 1 (*ΔcsgD*: 0.34 (± 0.92); *ΔcsgB*: 0.22 (±0.18). According to the CFU counts, the cellulose deficient strain *ΔbcsA* has most of its cells in the biofilm. However, we detected significantly larger impedance changes in the supernatant (BPI index 0.09 (± 0.14), which might be explained by flocculation. Overall the BPI index can thus be used to discriminate which effects (surface or supernatant) in the culture are more dominant.

3.3 Three-dimensional structure and spatial heterogeneity of wt, *ΔcsgD*, *ΔcsgB* and *ΔbcsA* mutants of *E. coli* TG1

Spatial heterogeneity is a crucial factor defining the complexity of bacterial biofilms and the challenges related to their eradication. Diversity in microbial populations has been shown to provide advantages for survival in adverse conditions for example in the presence of antimicrobials [39]. Traditionally, electrodes with large areas in the range of the mm^2 are used to study microbiological processes using impedance spectroscopy [33]. The size of these electrodes, however, does not allow to study physiological heterogeneity within the biofilm. The use of MEA chips, consisting of multiple electrodes with micro-scale dimensions, allows us to detect spatial heterogeneity within the *E.coli* TG1 biofilm with a resolution which is unprecedented for biofilm impedance spectroscopy. Figure 4 illustrates representative relative impedance changes as a color-coded spatial distribution on the MEA surface. As already touched upon above, the curli producing strains (WT and *ΔbcsA*) show a larger heterogeneity for both LF_{im} and LF_{re} compared to the curli deficient strains. For the specific chips illustrated in Figure 4, we found relative changes in LF_{im} ranging from -52,7% to -0.5% for the WT and changes from -7% to 0.8% for the Δ*bscA*. In contrast, *ΔcsgD* only ranges from -10 to -8.7% and *ΔcsgB* from -5.7 to -4.2%. Subtle heterogeneity of the biofilm could also be visualized by confocal laser scanning microscopy (CLSM) after staining the bacterial cells and extracellular polysaccharides (Suppl. Fig. 1). Consistent with the impedance measurements, CLSM indicated that cells of the curli producing strains cluster in tower-like structures, whereas the *ΔcsgD* and *ΔcsgB* biofilms rather represent a cellular monolayer. Nevertheless, in contrast to microscopic examination, MEA-based EIS measurements are label-free and non-invasive, and offer a spatial resolution as small as 100 µm. Here, we were able to detect very localized impedance effects that correspond to areas in the biofilm of stronger cellular attachment (larger LF_{re}) or higher concentrations of ions or electrolytes (smaller LF_{im}). EIS based heterogeneity thus represents another important parameter to aid discrimination between different biofilms. Further, the use of high-density silicon-based MEA chips, with electrode pitches down to 13 µm, could dramatically increase the spatial resolution and make EIS fingerprinting therefore even more sensitive [40].

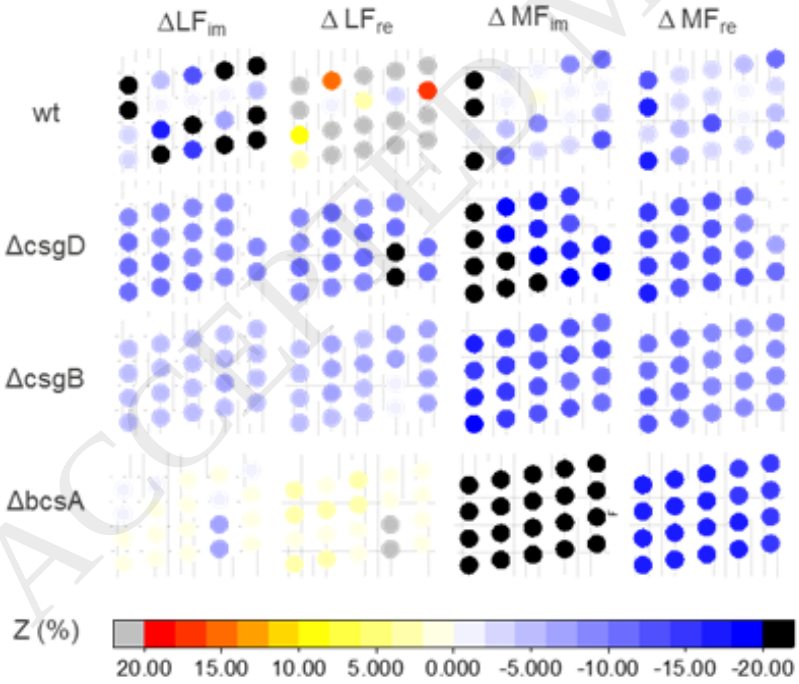

Figure 4. Structural characterization of WT, curli and cellulose deficient (*ΔcsgD*), curli deficient (*ΔcsgB*) and cellulose deficient (*ΔbcsA*) mutants. A-D) Spatial representation of LF_{im}, LF_{re}, MF_{im} and MF_{re}. recorded from MEA chips. Each individual point represents the relative impedance coded in agreement with the color map in the legend. Empty spaces

represent broken contacts. Each reticle shows one MEA chip. Refer to the supplementary figure 3 to see the color maps of the remaining chips measured.

3.4 Impedimetric characterization of WT, *ΔcsgD*, *ΔcsgB* and *ΔbcsA* mutants of *E. coli* TG1 along the biofilm growth curve

Biofilm maturation is a complex process that consists of different steps: (i) initial attachment, (ii) extracellular polysaccharide production, cell division and increased attachment and (iii) formation of three-dimensional structure [41]. At the latter time point the biofilm shows its maximum tolerance against antimicrobial treatment. The *E.coli* TG1 biofilm needs approximately 24 hours to maturate. In order to monitor the growth of the WT and knock-out mutants, we measured the impedance overtime for 24 hours.

The relative impedances for each time-lapse experiment are not normally distributed. Consequently, we believe that the most suitable way to represent the biofilm growth curves is by plotting the median. As a comparison, we measured the CFUs of both the biofilm and supernatant every 2 hours (Fig. 5E-F).

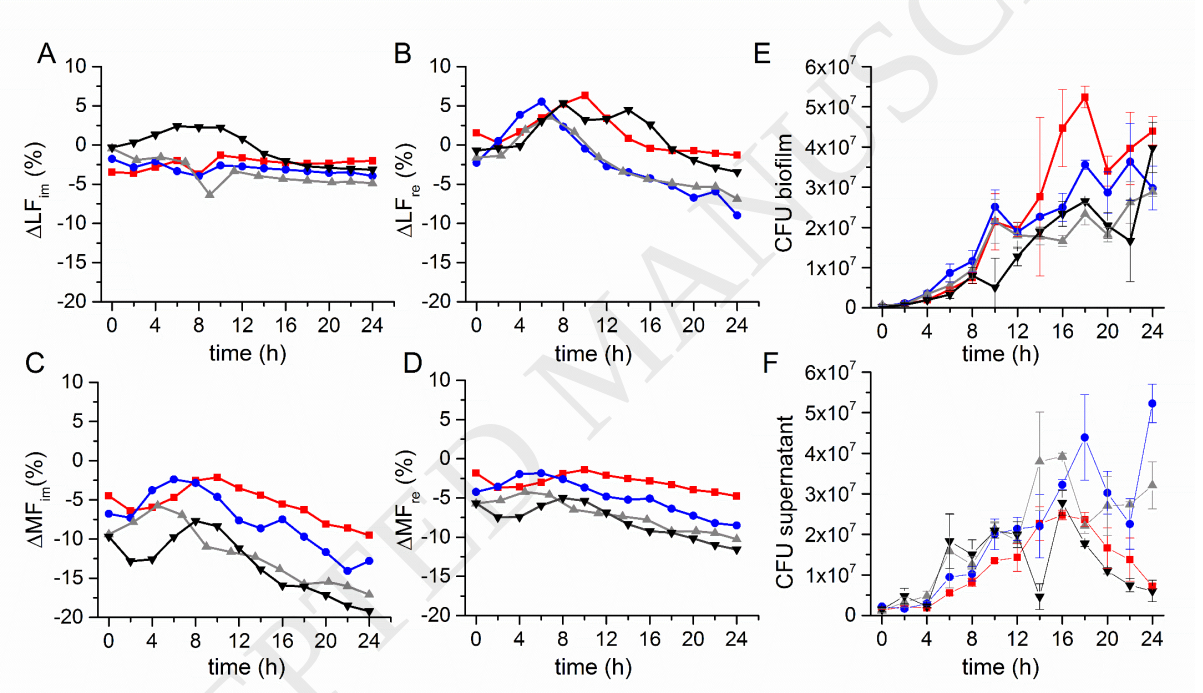

Figure 5. A-D Temporal impedance profile of WT (■), curli and cellulose deficient (*ΔcsgD* ■), curli deficient (*ΔcsgB* ■) and cellulose deficient (*ΔbcsA* ■) mutants along the biofilm growth curve; E-F. Temporal profile of colony forming units of the biofilm and the supernatants.

In each of the impedance profiles represented in Figure 5, two phases can be distinguished. In the initial phase (from 0 to 6 or 10h, depending on the strain) the impedance curves show the strongest differences between the strains (Fig. 5A-D). The largest changes in the parameters related to surface changes, i.e. LF_{im} and LF_{re}, take place during this initial phase (Fig. 5A, B). Consistently, parallel analyses of biofilm structure (confocal microscopy) indicate that it takes 10h for the WT to fully cover the electrode surface and only then the biofilm starts to mature into a three-dimensional structure (Suppl. Fig. 3). During the following maturation phase (10 to 24h), all the strains show linear impedance changes. The LF parameters show more subtle changes compared to the initial phase since the surface of the electrodes is already fully covered and the main changes are now seen in the MF values, the parameters related to the changes in the supernatant.

In the initial phase of biofilm attachment, the strains that produce curli proteins (WT and *ΔbcsA*, red and black trace, respectively) show an increase in LF_{im}, related to a decrease in electrode surface capacitance. During the first 10h the WT shows a slight increase in LF_{im}, from -3.4% to -1.3%. The cellulose deficient mutant (*ΔbcsA,* black trace) shows a sharp increase (up to 2.2%). A similar increase of the imaginary impedance in the first phase of growth at 1Hz was observed by Yang *et al*. For the curli deficient mutants we only observed decreases in LF_{im}, probably because the cells in this biofilm are less strongly attached. Consequently, the actual surface area is not reduced as much as for the WT and *ΔbcsA* mutant. The *ΔcsgD* mutant (blue trace) decreased from -1.7% to -3.9% and the *ΔcsgB* mutant (grey trace) from -0.45% to -4.9% probably due to changes in permittivity in the neighborhood of the electrode.

During this first phase also strong changes were observed in the interfacial resistance, LF_{re}. The changes in resistance at low frequencies during the initial biofilm growth have been previously reported to describe adsorption of organic compounds and attachment of bacterial cells [29,30]. We detected an increase of LF_{re} for all the strains, which is lasting longer for the strains with curli (10 hours for the WT (red trace) and 8 hours for the cellulose deficient *ΔbcsA* mutant, black trace) compared to the curli deficient strains (6 hours for both *ΔcsgD* and *ΔcsgB,* blue and grey trace respectively). We linearly fitted the impedance profile of LF_{re} during the initial phase and the slope then could be used to represent the attachment of extracellular matrix and cells. The strains that produce curli have a slower attachment slope (57% for WT and 77% for *ΔbcsA*, Supplementary info for fitting details) than the curli deficient strains (133% and 95% for *ΔcsgD* and *ΔcsgB* respectively). Similarly, we calculated the slope of the temporal CFU profile for the biofilm (Supplementary Table 1). This result confirms by CFU, that the WT is the slowest attaching strain, followed by Δ*bscA*, *ΔcsgB* and *ΔcsgD*.

The initial phase is also characterized by changes in the middle frequencies which are related to the activity in the supernatant. For both MF parameters the curli producing strains (WT red trace and *ΔbcsA* black trace) show the same curve shape (Fig. 5C and D). However, at the beginning of the biofilm lifecycle there is an offset of 5% between both strains. The lower initial values of the *ΔbcsA* mutant could possibly be related to incomplete separation (flocculation) of the cells already at inoculation, which might reduce the insulating effect of the cells. Initially, both WT and *ΔbcsA* decrease for 4 h in MF_{im} and MF_{re}. This change is related to an increase in permittivity and in conductivity, respectively. Both effects are presumably associated with the production of metabolites in the growth media [30,29]. Besides metabolite production, also bacterial cells keep on proliferating in the medium. Cells act as insulators and therefore block the passage of current and increase the impedance. We postulate therefore that the local minimum observed at 4 hours of growth is the result of an equilibrium between the effect of the ionic strength of the metabolites on the one hand and the insulating cells on the other hand. After 4 hours, the effect of the proliferating cells starts to dominate the impedance signal and results in an impedance increase that lasts until 8 hours of growth. At this time point, we observed a local maximum that resulting from a new equilibrium between the effect of cells and metabolites.

Initially, the strains lacking curli also show a similar curve shape for the MF parameters. In contrast with the decrease in MF parameters observed for WT and *ΔbcsA* mutant, *ΔcsgD* and *ΔcsgB* show an initial increase until 6 hours that corresponds to a higher number of unflocculated cells in the supernatant (Fig 5F).

During the maturation phase, starting at 10 hours, the effect of the metabolites is stronger than the effect of the cells. We could detect a linear decrease of the impedance for all the strains for LF_{re}, MF_{im} and MF_{re}, which relates to higher conductivity. The stronger decrease in superficial resistance (LF_{re}) observed for the curli-deficient strains (Fig. 5B) can be explained by the lower number of biofilm cells for these strains, which is associated with a lower insulating effect. Indeed, the number of biofilm cells of the *ΔcsgD* and *ΔcsgB* mutant only increased only up to $2.9x10^7$ and $2.8x10^7$ CFUs at

24 h, whereas the WT and *ΔbcsA* increased up to a $4.2x10^7$ and $3.9x10^7$ CFUs respectively (Fig. 5E). The level of impedance reduction in the middle frequencies (Fig. 5C-D) on the other hand could not be correlated to changes in supernatant CFUs (Fig 5. F). As previously reported in the literature [29,30,33], the impedance in the medium frequencies appears to be more sensitive to metabolic activity rather than to the actual number of cells present. An exception is the strong decrease in MF_{im} and MF_{re} of the *ΔbcsA* mutant, which could possibly -at least in part be- explained by reduced insulation by cell flocculation. To improve the understanding of the temporal impedance profiles, it would be interesting to follow metabolite production (acetate, ammonia, lactate…) for the different strains.

4. Conclusions

In this study we used MEA chips to compare impedance fingerprints of the WT and the isogenic *ΔcsgD*, *ΔcsgB* and *ΔbcsA* mutants of the well-known *Escherichia coli* TG1 biofilm. After 24h of growth all the strains showed surface related impedance changes. Firstly, we observed an increase in capacitance and thus permittivity of the double layer of the electrode. Next, an increase in the interfacial resistance was only observed for the curli producing strains, proving that these strains block more current than non-curli producing films. In the middle frequencies, which relate to supernatant effects, we observed a decrease in impedance caused by the increase in ionic strength due to metabolite production. The cellulose deficient mutant shows a larger decrease in impedance and we postulate that this is due to flocculation in the medium.

Furthermore, compared to previous impedance sensors for bacterial sensing, the use of MEAs allows to gather detailed spatial information that can be related to physiological heterogeneity in the biofilm, and can therefore aid classification of biofilms. We observed for instance that the impedance recorded from the different chip electrodes is most variable for the WT biofilm. This heterogeneity was confirmed by confocal images.

Finally, we showed the utility of impedance spectroscopy to characterize the biofilm life-cycle of the strains under investigation. We observed two phases in the temporal impedance profiles: the initial phase, presumably related to attachment, lasts between 6 to 10h, and is followed by a maturation phase. The attachment phase is mainly characterized by an increase in the interfacial resistance. The attachment slope calculated from the impedance profile is consistent with the slope calculated based on CFU counts. The maturation phase on the other hand is mainly characterized by a decrease in the middle frequencies, which relates to increased conductivity.

Altogether, impedance spectroscopy using MEA chips with small electrode pitch is a powerful, non-invasive and label-free technique to discriminate between isogenic biofilms, and gives information about surface and supernatant effects, as well as biofilm heterogeneity. Impedance sensors are promising tools for detection of biofilms in industrial and clinical applications.

Acknowledgements

This research was funded by the CREA/13/020 project from the KU Leuven, Belgium and by the IWT Flanders under the grant agreement SBO NEMOA (I-SBO 120050) and by FWO-Vlaanderen (W0.020.11 N). H. S. is grateful for receiving a post-doctoral fellowship from the FWO-Vlaanderen. The authors would like to thank Jordi Cools for taking the SEM pictures.

References

1. Hoiby, N., Bjarnsholt, T., Givskov, M., Molin, S. & Ciofu, O. Antibiotic resistance of bacterial biofilms. *Int J Antimicrob Agents* **35,** 322–332 (2010).

2. Flemming, H.-C. & Wingender, J. *Biofilm Highlights*. (Springer Berlin Heidelberg).

3. Hetrick, E. M. & Schoenfisch, M. H. Reducing implant-related infections: active release strategies. *Chem. Soc. Rev.* **35,** 780–9 (2006).

4. Fux, C. a, Costerton, J. W., Stewart, P. S. & Stoodley, P. Survival strategies of infectious biofilms. *Trends Microbiol.* **13,** 34–40 (2005).

5. Strathmanna, M., Mittenzweyb, K.-H., Sinnc, G., Wassilios, P. & Flemming, H.-C. Simultaneous monitoring of biofilm growth, microbial activity, and inorganic deposits on surfaces with an in situ, online, real-time, non-destructive, optical sensor. *Biofouling J. Bloadhesion Biofilm Res.* **Volume 29,** (2013).

6. Ahmed, A., Rushworth, J. V, Hirst, N. a & Millner, P. a. Biosensors for whole-cell bacterial detection. *Clin. Microbiol. Rev.* **27,** 631–46 (2014).

7. Janknecht, P. & Melo, L. F. Online biofilm monitoring. *Rev. Environ. Sci. Biotechnol.* 269–283 (2004).

8. Kirschhöfer, F. *et al.* Quartz crystal microbalance with dissipation coupled to on-chip MALDI-ToF mass spectrometry as a tool for characterising proteinaceous conditioning films on functionalised surfaces. *Anal. Chim. Acta* **802,** 95–102 (2013).

9. Reipa, V., Almeida, J. & Cole, K. D. Long-term monitoring of biofilm growth and disinfection using a quartz crystal microbalance and reflectance measurements. *J. Microbiol. Methods* **66,** 449–459 (2006).

10. Cheng, J.-H. & Sun, D.-W. Recent Applications of Spectroscopic and Hyperspectral Imaging Techniques with Chemometric Analysis for Rapid Inspection of Microbial Spoilage in Muscle Foods. *Compr. Rev. Food Sci. Food Saf.* **14,** 478–490 (2015).

11. Lisdat, F. & Schäfer, D. The use of electrochemical impedance spectroscopy for biosensing. *Anal. Bioanal. Chem.* **391,** 1555–67 (2008).

12. Barsoukov, E. & Macdonald, J. R. *Impedance Spectroscopy Theory, Experiment, and Applications*. (2005).

13. Paredes, J., Becerro, S. & Arana, S. Comparison of real time impedance monitoring of bacterial biofilm cultures in different experimental setups mimicking real field environments. *Sensors Actuators B Chem.* **195,** 667–676 (2014).

14. Paredes, J. *et al.* Interdigitated microelectrode biosensor for bacterial biofilm growth monitoring by impedance spectroscopy technique in 96-well microtiter plates. *Sensors Actuators B Chem.* **178,** 663–670 (2013).

15. Paredes, J. *et al.* Real time monitoring of the impedance characteristics of Staphylococcal bacterial biofilm cultures with a modified CDC reactor system. *Biosens. Bioelectron.* **38,** 226–32 (2012).

16. Bayoudh, S., Othmane, A., Ponsonnet, L. & Ben Ouada, H. Electrical detection and characterization of bacterial adhesion using electrochemical impedance spectroscopy-based flow chamber. *Colloids Surfaces A Physicochem. Eng. Asp.* **318,** 291–300 (2008).

17. Pires, L. *et al.* Online monitoring of biofilm growth and activity using a combined multi-channel impedimetric and amperometric sensor. *Biosens. Bioelectron.* **47,** 157–163 (2013).

18. Bruchmann, J., Sachsenheimer, K., Rapp, B. E. & Schwartz, T. Multi-Channel Microfluidic Biosensor Platform Applied for Online Monitoring and Screening of Biofilm Formation and Activity. *Plos* 1–19 (2015). doi:10.1371/journal.pone.0117300

19. Muñoz-Berbel, X., Muñoz, F. J., Vigués, N. & Mas, J. On-chip impedance measurements to monitor biofilm formation in the drinking water distribution network. *Sensors Actuators, B Chem.* **118,** 129–134 (2006).

20. Muñoz-Berbel, X., García-Aljaro, C. & Muñoz, F. J. Impedimetric approach for monitoring the formation of biofilms on metallic surfaces and the subsequent application to the detection of bacteriophages. *Electrochim. Acta* **53,** 5739–5744 (2008).

21. Ward, A. C., Connolly, P. & Tucker, N. P. Pseudomonas aeruginosa can be detected in a polymicrobial competition model using impedance spectroscopy with a novel biosensor. *PLoS One* **9,** e91732 (2014).

22. Obien, M. E. J., Deligkaris, K., Bullmann, T., Bakkum, D. J. & Frey, U. Revealing neuronal function through microelectrode array recordings. *Front. Neurosci.* **8,** 1–30 (2015).

23. Jahnke, H.-G. *et al.* Impedance spectroscopy based measurement system for quantitative and label-free real-time monitoring of tauopathy in hippocampal slice cultures. *Biosens. Bioelectron.* **32,** 250–8 (2012).

24. Jahnke, H. G. *et al.* Impedance spectroscopy-An outstanding method for label-free and real-time discrimination between brain and tumor tissue in vivo. *Biosens. Bioelectron.* **46,** 8–14 (2013).

25. White, A. P., Gibson, D. L., Kim, W., Kay, W. W. & Surette, M. G. Thin aggregative fimbriae and cellulose enhance long-term survival and persistence of Salmonella. *J. Bacteriol.* **188,** 3219–3227 (2006).

26. Solano, C. *et al.* Genetic analysis of Salmonella enteritidis biofilm formation: Critical role of cellulose. *Mol. Microbiol.* **43,** 793–808 (2002).

27. Welkenhuysen, M. *et al.* An integrated multi-electrode-optrode array for in vitro optogenetics. *Sci. Rep.* **6,** 20353 (2016).

28. Valdivia, R. H. & Falkow, S. Fluorescence-based isolation of bacterial genes expressed within host cells. *Science* **277,** 2007–11 (1997).

29. Felice, C. J., Valentinuzzi, M. E., Vercellone, M. I. & Madrid, R. E. Impedance bacteriometry: Medium and interface contributions during bacterial growth. *IEEE Trans. Biomed. Eng.* **39,** 1310–1313 (1992).

30. Yang, L., Ruan, C. & Li, Y. Detection of viable Salmonella typhimurium by impedance measurement of electrode capacitance and medium resistance. *Biosens. Bioelectron.* **19,** 495–502 (2003).

31. Karnaushenko, D. *et al.* Monitoring microbial metabolites using an inductively coupled resonance circuit. *Sci. Rep.* **5,** 12878 (2015).

32. John, A. & Cole, W. H. Studies on Bacterial Metabolism ’. *J. Bacteriol.* 571–586 (1938).

33. Varshney, M. & Li, Y. Interdigitated array microelectrodes based impedance biosensors for detection of bacterial cells. *Biosens. Bioelectron.* **24,** 2951–60 (2009).

34. Steenackers, H., Hermans, K., Vanderleyden, J. & Keersmaecker, S. C. J. De. Salmonella bio fi lms : An overview on occurrence , structure , regulation and eradication. *FRIN* **45,** 502–531 (2012).

35. Flemming, H.-C. & Wingender, J. The biofilm matrix. *Nat. Rev. Microbiol.* **8,** 623–633 (2010).

36. Brombacher, E., Baratto, A., Dorel, C. & Landini, P. Gene expression regulation by the Curli activator CsgD protein: modulation of cellulose biosynthesis and control of negative determinants for microbial adhesion. *J. Bacteriol.* **188,** 2027–37 (2006).

37. Re, S. Da & Ghigo, J. A CsgD-Independent Pathway for Cellulose Production and Biofilm Formation in Escherichia coli A CsgD-Independent Pathway for Cellulose Production and Biofilm Formation in Escherichia coli †. **188,** 3073–3087 (2006).

38. Paredes, J., Becerro, S. & Arana, S. Comparison of real time impedance monitoring of bacterial biofilm cultures in different experimental setups mimicking real field environments. *Sensors Actuators B Chem.* **195,** 667–676 (2014).

39. Stewart, P. S. & Franklin, M. J. Physiological heterogeneity in biofilms. *Nat. Rev. Microbiol.* **6,** 199–210 (2008).

40. Dragas, J. *et al.* In Vitro Multi-Functional Microelectrode Array Featuring 59 760 Electrodes, 2048 Electrophysiology Channels, Stimulation, Impedance Measurement, and Neurotransmitter Detection Channels. *IEEE J. Solid-State Circuits* **52,** 1576–1590 (2017).

41. Stoodley, P., Sauer, K., Davies, D. G. & Costerton, J. W. Biofilms as complex differentiated communities. *Annu. Rev. Microbiol.* **56,** 187–209 (2002).

Parameter		Interpretation
LF_{im}	Z_{im} (2Hz)	$-j/\omega C_{dl}$; $C_{dl}=\varepsilon_{dl}A/d$
LF_{re}	Z_{re} (2Hz)	R_{int}
MF_{im}	Z_{im} (5kHz)	$-j/\omega C_m$
MF_{re}	Z_{re} (5kHz)	R_m

Table 1. Summary of impedance parameters used for the interpretation of the biofilm grown on the MEA chips. LF_{im} is the imaginary impedance at 2Hz and is inversely proportional to the double layer capacitance of the electrode, C_{dl}. The double layer capacitance depends on the permittivity of the double layer (ε_{dl}), active area of the electrodes (A) and the distance of the layer, d. LF_{re} is the real impedance at 2Hz and corresponds to the apparent interface resistance R_{int}. MF_{im} is linked to the apparent medium capacitance (C_m) and MF_{re} refers to the medium resistance, R_m.

	LF_{im}	LF_{re}	MF_{im}	MF_{re}	BPI
WT (curli+/cellulose+)	↓	↑↑	↓	↓	1.47 (± 4.87)
***ΔcsgD* (curli-/cellulose-)**	↓	↓	↓	↓	0.34 (± 0.92)
***ΔcsgB* (curli-/cellulose+)**	↓	↓	↓	↓	0.22 (± 0.18)
***ΔbcsA* (curli+/cellulose-)**	↓	↑	↓↓	↓↓	0.09 (± 0.14)

Table 2. Summary of impedance parameters for the WT, *ΔcsgD, ΔcsgB* and *ΔbcsA* biofilms. LF_{im} shows the relative changes in the imaginary impedance at low frequencies. This changes are inversely proportional to the double layer capacitance of the electrode-electrolyte interface. LF_{re} are the changes in the real impedance at low frequencies and it relates to the electrode interfacial resistance. MF_{im} and MF_{re} represent the changes in the medium capacitance and resistance, respectively.